Contents list available at IJRED website

International Journal of Renewable Energy Development

Journal homepage: https://ijred.undip.ac.id

Research Article

Thermal Performance of Double Pass Solar Air Heater With Tubular Solar Absorber

Nassr Fadhil Hussein[a*], Sabah T. Ahmed[b], Ali L. Ekaid[a]

[a]*Mechanical Engineering Department, University of Technology-Iraq*

[b]*Department of Aeronautical Engineering Technology, Bilad Alrafidain University College, Diyala, 32001, Iraq*

Abstract. In this investigation, the effect of replacing the conventional solar absorber with a new solar absorber on the thermal performance of a double-pass solar air heater has been studied experimentally and numerically. Three configurations have been introduced, the first configuration is a double pass solar air heater with a flat plate solar absorber (DPSAHWFP) for the aim of comparison, and the second configuration is a double pass solar air heater with a tubular absorber that includes a set of tubes which are fitted perpendicularly to the direction of airflow (DPSAHWT-1), and the third configuration is double-pass solar air heater with a tubular absorber that involves set of tubes which are fitted in parallel to the direction of airflow (DPSAHWT-2). The experiments have been carried out under indoor conditions at a constant heat flux equal to 1000 W/m^2 and different air mass flow rates (0.01– 0.03 kg/s). The results revealed that the air mass flow rate has a substantial impact compared to the rise in air temperature, hence, the thermal performance of solar air heater is directly proportional to increase air mass flow rate. In addition, the experimental and numerical outcomes indicated that for all air flow rates. The (DPSAHWT-2) offers higher thermal performance as compared to other models, where the maximum effective efficiency has been obtained at 0.03 kg/s equal to 80.9 %. Moreover, (DPSAHWT-2) is more efficient than DPSAHWFP and DPSAHWT-1 by 4.2 % and 9.8 % respectively.

Keywords: Solar air heaters, heat transfer, double pass, thermal performance, tubular absorber.

Received: 22nd May 2022; Revised: 17th July 2022; Accepted: 26th August 2022; Available online: 24th Sept 2022

1. Introduction

Recently, many countries paid attention to investing in the renewable energy sector as an attempt to reduce the consumption of fossil fuels and the consequences of burning these types of fuels such as pollutants that harm human beings and plants (Jasim Mahmood 2020). Solar energy is the most available source among other renewable energy sources, in addition to that, it is free, clean, eco-friendly, and inexhaustible (Kumar *et al.* 2021a). Investing in the solar energy field contributes to minimizing CO_2 levels and global warming since the systems that are used for converting solar irradiance into other's energy forms produce no pollutants (Khanmohammadi *et al.* 2021). Solar energy can be converted directly into electricity via photovoltaic panels (Monna *et al.* 2022) or into heat via many systems such as solar air heaters (SAHs) (Jalil *et al.* 2021), solar water collectors (Shafiee *et al.* 2022), solar chimneys (Karimipour-Fard and Beheshti 2017), etc. Solar air heaters are utilized in many applications such as supplying hot air in agriculture dryers for drying agricultural crops and fruits as well as supplying hot air in buildings especially in the winter season to make it comfortable for living (Razak *et al.* 2016). Solar air heaters (SAHs) are characterized by simplicity of design and low cost compared to other systems (Rajarajeswari *et al.* 2018). However, SAHs are not complete systems like other systems, they suffer from some weaknesses that can be represented as follows: firstly, low system efficiency due to the weak heat transfer between airflow and solar absorber due to low heat capacity of air; secondly, the energy losses represented by (optical, convection, radiation and conduction); and finally, the intermittency of solar energy during the cloudy sky and nighttime (Salih *et al.* 2019a). Many efforts represented by research have been done to overcome these weaknesses and offered lots of solutions. Regarding energy losses, different technologies were used. Abdelkader *et al.* (2020) utilized CNTs and CuO nanoparticles to enhance the optical properties of black paint via enhancing surface roughness and surface spectral selectivity. The thermal efficiency was enhanced up to 24.4% compared with ordinary black paint case when using just 4% from CNTs/ CuO nanoparticles. Kumar *et al.* (2019b) investigated the effect of insulation types on reducing conduction energy losses, and they prevailed that ceramic wool is the best material among the tested materials for reducing conduction energy losses and improving thermal efficiency. Dhiman *et al.* (2012) mentioned that utilizing double or multi-transparent covers at the top side of the collector can prevent most of the long-wave radiation from escaping to the outside surrounding. Regarding the solar irradiance intermittency problem, lots of researchers focused on solving this problem by integrating solar air heaters with different designs of thermal energy storage systems. For example, Assadeg *et al.* (2021) used a new design of a double-pass solar air heater and integrated it

* Corresponding author:
Email: 50153@uotechnology.edu.iq (N.F.Hussein)

https://doi.org/10.14710/ijred.2023.46328
ISSN: 2252-4940/© 2023.The Author(s). Published by CBIORE

with a built-in latent heat thermal energy storage system which is involved fins. The results revealed that the proposed system has the ability to increase thermal efficiency up to 73%. Habib *et al.* (2020) used a mixture of 3% of single-wall carbon nanotubes and paraffin wax as a hybrid latent thermal energy storage system. It was found that utilizing the paraffin nanocomposite improved the thermal storage efficiency by about 20.7% and 21.2% for natural and forced operating conditions respectively. Abd (2016) studied the effect of using a combination of latent and sensible thermal energy storage materials on the thermal performance of the double-pass solar air heater. The study findings indicated the ability of the latent-sensible mixture to allow the solar heater to work for 380 min during the discharge period. For improving the heat transfer rate between airflow and solar absorber, the researchers used different ways and methods such as creating artificial roughness on the solar absorber surface (Das *et al.* 2020; Kanase *et al.* 2022), utilizing turbulators like dimples (Salman *et al.* 2022; Perwez *et al.* 2019), baffles (Abdu 2021; Rajendran *et al.* 2021), fins (Erol 2022; Saboohi *et al.* 2022), winglets (Kumar *et al.* 2021b), etc., or replacing the conventional flat solar absorber by novel configurations of absorbers for the purpose of increasing contact surface area, and hence improving the thermal efficiency, for instance, Khanlari *et al.* (2020) replaced the conventional plate with a V-groove absorber and enhanced the thermal efficiency up to about 81%. Ho *et al.* (2020) used a sinusoidal corrugated plate as an alternative to a conventional plate absorber and achieved an increment in thermal efficiency up to about 70.3%. Mohammed *et al.* (2021) improved the thermal efficiency within a range of 63.7 -74.2% by replacing the conventional plate with a triangular absorber plate and metallic fiber. Akhbari *et al.* (2020) utilized triangular channels to enhance the thermal performance by about 45.27%, Gopi *et al.* (2021) used a photovoltaic panel integrated with slats from underneath instead of the conventional absorber plate and raised the energy efficiency up to 58.24%, Singh *et al.* (2021) used a combination of wavy channel and porous media as a solar absorber, and they achieved an enhancement in thermal performance of about 38 to 93%. Abo-Elfadl *et al.* (2021a) proposed a new type of solar absorber that included a set of tubes and enhanced the thermal efficiency up to 133%.

Recently, using novel solar absorbers as an alternative to the conventional flat plate absorber has become an interesting research idea. However, this technique is still under development and needs more investigation. Thus, the present work offers a novel design of solar absorbers involving a set of tubes with a circular cross-section as an alternative to the conventional flat plate absorber and studying the effect of the orientation of the tube relative to the airflow direction on thermal performance experimentally and numerically.

2. Numerical Analysis steps

2.1. Geometry and meshing

The modeling of proposed solar air heaters was done by using CFD software ANSYS fluent version (2021 R2). The geometry of double pass solar air heater with flat plate absorber (DPSAHWFP), double pass solar air heater with horizontal tubes (DPSAWT-1), and double pass solar air heater with longitudinal tubes (DPSAHWT-2) which are included the transparent cover layer, backplate, absorber tubes, side, and bottom insulations are made by designed modeler of ANSYS workbench 2021 R2. The generated models are presented in Figs. 1a to 1c. The collector's projected area is 1200 × 300 mm.

The meshing tool in ANSYS workbench 2021 R2 is used to perform meshing for the configurations as shown in Fig. 2. Structured mesh is generated, and the dependency of mesh on the solution's accuracy was achieved by doing an independent mesh test, where the mesh concentration is increased gradually until the variation in outlet temperature becomes less than 1%.

2.2 Governing equations

The governing equations that are utilized to determine the velocity, pressure, and temperature are the continuity, momentum, and energy equations (Alic *et al.* 2021; Heydari and Mesgarpour 2018).
Continuity equation:

$$\nabla.(\rho\vec{v}) = 0 \quad (1)$$

Momentum conservation equations:

$$\frac{\partial}{\partial t}(\rho\vec{v}) + \nabla.(\rho\vec{v}\vec{v}) = -\nabla.P + \nabla.(\vec{\tau}) + \rho\vec{g} \quad (2)$$

Energy conservation equation:

$$\frac{\partial}{\partial t}(\rho E) + \nabla.(\vec{v}(\rho E + P)) = \nabla.\left(k_{eff}\nabla.T\right) \quad (3)$$

Where, (ρ) represents the density of the fluid, (v) represents the fluid flow velocity, (*P*) represents the static pressure, (ρg) represents the gravitational force, (E) represents the total energy of fluid, τ represents the shear tensor, and (k_{eff}) represents the effective conductivity (Singh *et al.* 2021).

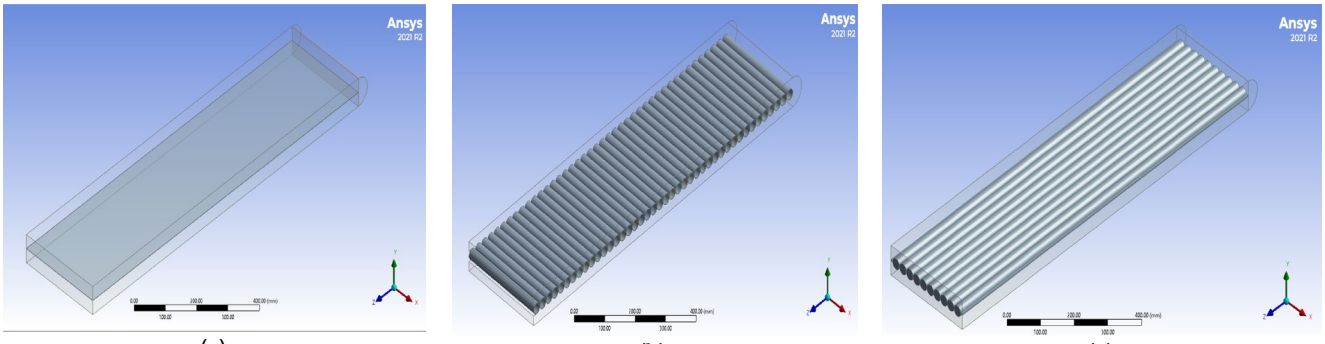

(a) (b) (c)

Fig. 1. (a) The geometry of DPSAHF, (b) The geometry of DPSAHWT-1, (c) The geometry of DPSAHWT-2.

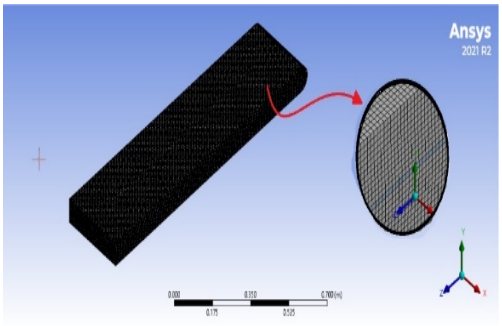

Fig. 2. The meshing of the 3D model.

The governing equations have been solved by using the finite-volume method and the pressure-based solver. In addition, A semi-implicit pressure-linked algorithm (SIMPLE) has been adopted for the purpose of pressure velocity coupling. Moreover, for discretizing the governing equations, a second-order upwind scheme is applied. For simulating flow as well as heat transfer, the renormalization group (RNG)- k-ε model has been selected since this model as well as both the Blasius empirical correlation and the Dittus-Boelter empirical correlation have approximately the same results (Yadav and Bhagoria 2013). The following transport equations were used to solve the turbulence kinetic energy and turbulence dissipation rate (BENSACI 2021):

$$\frac{\partial(\rho k)}{\partial t}+\frac{\partial(\rho k u_i)}{\partial x_i}=\frac{\partial}{\partial x_j}\left[\alpha_k \mu_{eff}\frac{\partial k}{\partial x_j}\right]+G_k+G_b-\rho\varepsilon \quad (4)$$

$$\frac{\partial(\rho \varepsilon)}{\partial t}+\frac{\partial(\rho \varepsilon u_i)}{\partial x_i}=\frac{\partial}{\partial x_j}\left[\alpha_\varepsilon \mu_{eff}\frac{\partial \varepsilon}{\partial x_j}\right]+C_{1\varepsilon}\frac{\varepsilon}{k}(G_k+C_{3\varepsilon}G_b)-2C_{2\varepsilon}\rho\frac{\varepsilon}{k}-R_\varepsilon \quad (5)$$

Where, (k) represents the turbulence kinetic energy, (ε) represents the turbulence dissipation rate, (G_k) and (G_b) represent the generation of turbulence kinetic energy due to the mean velocity gradients and buoyancy respectivialy. In the above equations, Cμ= 0.0845, $\alpha_k = \alpha_k$ =1.393, $C_{1\varepsilon}$ = 1.42, $C_{2\varepsilon}$ =1.68, and $C_{3\varepsilon}$ =1.8. The term (R_ε) which represents the main difference between the standard and renormlized group k-ε models can be expressed by the following formula:

$$R_\varepsilon=\frac{\rho C_\mu \frac{\eta^3}{\varepsilon}\varepsilon^2\left(1-\frac{\eta}{\eta_o}\right)}{1+\beta\eta^3} \quad (6)$$

Where, β=0.012, η_o= 4.38, and $\eta = Sk/\varepsilon$.
The convergence criteria for continuity, momentum, and energy equations are set to 1e-03 and 1e-06 respectively.

2.3 Assumptions

- Working fluid flow is assumed incompressible, and the type of case is 3D.
- The airflow through the lower & upper channels is assumed forced convection turbulent flow.
- Thermo-physical characteristics of the working fluid are assumed constant.
- No slip condition is assumed for the airflow at the wall
- The fluid inside the tubular capsules is assumed air with constant thermo-physical characteristics.

Table 1
Boundary conditions and operating parameters.

Boundary condition	Value
Solar rate	1000 W/m^2
Mass flow rate	0.01, 0.015, 0.02, 0.025 and 0.03 kg/s.
Inlet air temperature	25 ^{0}C
Wind velocity	1 m/s

Table 2
Glass cover, backplate, and absorber properties.

Glass cover	Density	2540.4 kg/m3
	Thermal conductivity	1.4 W/m.k
	Specific heat	770 J/kg.k
Backplate	Density	8013 kg/m3
	Thermal conductivity	80 W/m.k
	Specific heat	450 J/kg.k
Absorber	Density	8978 kg/m3
	Thermal conductivity	387.6 W/m.k
	Specific heat	381 J/kg.k
	Absorptivity	0.944

- Solar rate is uniform and equal to 1000 W/m^2.
- Back and side walls are assumed insulated (adiabatic walls).
- Outlet pressure condition is assumed atmospheric pressure, and the inlet thermal conditions is assumed equal to 25 ^{0}C.

2.4 Boundary conditions and operating parameters:

The boundary conditions that are used in the simulation are mentioned in Table 1. Moreover, the properties of both glass cover, backplate, and absorber tubes are mentioned in Table 2.

3 Experimental setup

3.1 General description

The solar air heater which is used in the experimental setup consists of the following main components: the first component is a transparent cover which is made from 4 mm glass material with a transmittance of 88% to allow the maximum rate of solar irradiance to pass through it and prevent longwave radiation to escape from the solar absorber to the surrounding, the second component is the solar absorber which is utilized to convert the incident solar energy into thermal energy.

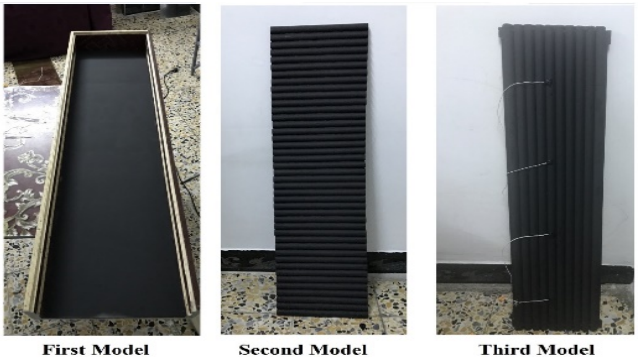

Fig. 3. Solar absorber models.

Table 3.
Dimensions and specifications of solar absorber models.

Model	Details
First model	Material type: Copper. Length: 1200 mm. Width: 300mm. Thickness:0.9 mm.
Second model	Material type: Copper. Length: 300 mm. Outer Diameter: 28.6 mm. Inner Diameter: 26.7 mm. Thickness: 0.9 mm. Number of tubes: 42 tubes.
Third model	Material type: Copper. Length: 1200 mm. Outer Diameter: 28.6 mm. Inner Diameter: 26.7 mm. Thickness: 0.9 mm. Number of tubes: 10 tubes.

Three configurations of the solar absorber as shown in Fig. 3 were used for the purpose of investigating the influence of tubes' direction with respect to the airflow direction namely: the first model involved using flat plate absorber as a reference (DPSAHWFP), the second model involved using a tubular absorber that is placed perpendicularly to the direction of airflow (DPSAHWT-1), and the third model involved using a tubular absorber that is placed in parallel to the direction of airflow (DPSAHWT-2).

The dimensions and specifications of the three solar absorber configurations are described in Table 3. The third main component of the solar air heater is the wood box which represents the solar air heater's body, this box is made from plywood material with dimensions and specifications that are mentioned in Table 4. The plywood box has been insulated from the sides and bottom with Polyurethane foam with a thickness of 50 mm. The reason for selecting Polyurethane foam is its low thermal conductivity. Moreover, galvanized plate with 1 mm thickness has been used in the lower channel with the aim of investing some of the thermal losses. The schematic diagram and photograph of the experimental setup are shown in Figs. 4a and b. .

Table 4.
Dimensions and specifications of the solar air heater body.

Model	Details
DPSAHWFP	Total length: 1260 mm. Total width: 340mm. Total hight:80.9 mm. Effective length:1200 mm Effective width:300 mm Upper channel height: 40 mm Lower channel height: 40 mm
DPSAHWT-1	Total length: 1260 mm. Total width: 340mm. Total hight:80.9 mm. Effective length:1200 mm Effective width:300 mm Upper channel height:32.15mm Lower channel height:32.15mm
DPSAHWT-2	Total length: 1260 mm. Total width: 340mm. Total hight:80.9 mm. Effective length:1200 mm Effective width:300 mm Upper channel height:32.15mm Lower channel height:32.15mm

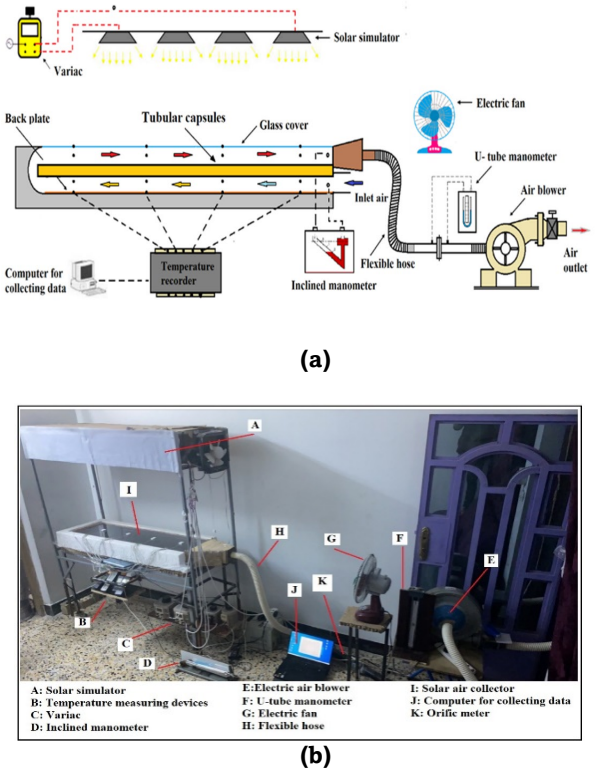

Fig. 4. (a) Schematic diagram of the experimental setup, (b) Photograph of the experimental setup.

The experiments are performed under indoor conditions. The artificial solar rate was achieved by using a solar simulator which is controlled via variac transformation for purpose of adjusting the solar rate to 1000 W/m^2. Furthermore, the turbulent flow is achieved by using an electric air blower. The air mass flow rates inside the solar air heater duct are ranged between (0.01-0.03) kg/s with an increment of 0.005 kg/s by using a manual valve that is located on the pumping side of the blower. The flow direction is set from the lower channel to the upper channel. The pressure difference through the solar heater is measured by connecting the measuring device to two tapes which are fixed at the inlet and outlet of the test section. The temperature distribution along both the glass cover, solar absorber, backplate, and upper and lower channels are measured by fitting four thermocouples type k in each part. Moreover, the inlet and outlet temperatures are measured by using two thermocouples that are fitted in the inlet and outlet. The positions of measuring points are shown in Fig. 5.

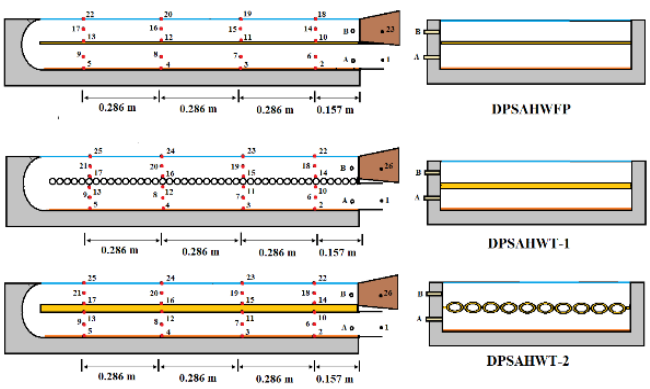

Fig. 5. Positions of measuring points.

Table 5
Details and specifications of instruments and measuring devices.

Instrument type	Model	Purpose of usage	Accuracy level
Solar power meter	SPM-1116SD	Measuring solar intensity	± 5 %
Orifice meter + U tube manometer	-	Measuring mass flow rate	±5 %
Data acquisition	MC-4244r2	Measuring temperatures	±0.1 0C
Digital thermometer	HT-9815	Measuring temperatures	±2 0C
Inclined manometer	-	Measuring pressure drop	± 2 %

3.2 Instruments and measuring devices

The details and specifications of instruments and measuring devices that are used in experiments are mentioned in Table 5.

3.3 Experimental procedure and data analysis

3.3.1 Experimental procedure

At the beginning of each experiment, the temperature of each thermocouple should give the same temperature as the room. Then, the air blower, as well as the solar simulator are switched on and regulated to maintain the desired value by using a control valve and voltage regulator. After that, the test rig runs until reaching a steady state, and during the running period, the temperatures of all thermocouples are measured every 5 minutes. Finally, when the steady state is achieved after 1 hour, the pressure drop across the solar air heater as well as all temperatures are recorded. After that, the solar simulator is switched off and the inlet and outlet temperatures are recorded every 5 minutes until the temperature difference between them equals approximately zero. The procedure is repeated by changing the airflow rate and fixing solar intensity or by changing both to another desired value within the test range.

3.3.2. data analysis

Depending on the first law of thermodynamics, the solar air heater's performance can be evaluated by the following formula (El-Sebaii *et al.* 2011):

$$\eta_{th} = \frac{Q_{out}}{Q_{in}} \quad (7)$$

Were Q_{out} and Q_{in} represent the useful energy gain from solar air heater and received energy which can be represented by the following formulas:

$$Q_{out} = \dot{m}_{air} . Cp_{air}(T_{air,out} - T_{air,in}) \quad (8)$$

$$Q_{in} = A_c . I \quad (9)$$

The term thermo-hydraulic efficiency or effective efficiency is used to take into account the influence of pressure drop on the solar air heater performance which can be calculated as follows (Hussein and Farhan 2019):

$$\eta_{eff} = \frac{Q_{out} - Q_{mechanical}}{Q_{in}} \quad (10)$$

Table 6
Uncertainty for measurements in the experimental part.

Parameters	Uncertainty
Mass flow rate	22.85673 - 71.28343 ±
Solar radiation	0.000649 - 0.000809 ±
Temp. difference	0.027972- 0.083917 ±
Pressure drop	7.18E-05 - 2.39E-05 ±
Effective efficiency	0.072354 - 0.177318 ±

$$Q_{mechanical} = \frac{\dot{m}_{air} \times \Delta p}{\rho_{air}} \quad (11)$$

Where, Q mechanical is a pumping power that is used for recycling air through the double pass solar air heater.

3.4 Uncertainty analysis

In general, any experimental work should have uncertainty analysis for purpose of indicating the possible error values in measurement instruments. The uncertainty values can be computed by the following the formula (Salih *et al.* 2021b):

$$W_R = \left[\left(\frac{\partial R}{\partial x_1} W_1\right)^2 + \left(\frac{\partial R}{\partial x_2} W_2\right)^2 + \cdots + \left(\frac{\partial R}{\partial x_n} W_n\right)^2\right]^{\frac{1}{2}} \quad (12)$$

Where: WR represents total uncertainty and (W1, W2, … Wn) represent the uncertainty of independent variables (x1, x2, …, xn).
Depending on eq-6 the uncertainty of effective efficiency can be written as follows:

$$W_{\eta eff} = \left[\left(\frac{\partial \eta eff}{\partial \dot{m}_a} W_{\dot{m}_a}\right)^2 + \left(\frac{\partial \eta eff}{\partial I_{solar}} W_{I_{solar}}\right)^2 + \left(\frac{\partial \eta eff}{\partial \Delta T} W_{\Delta T}\right)^2 + \left(\frac{\partial \eta eff}{\partial \Delta P} W_{\Delta P}\right)^2\right]^{\frac{1}{2}} \quad (13)$$

The uncertainty of measurements and effective efficiency have been presented in Table 6.

4 Results and Discussion

This section presents the outcomes of experimental and numerical works. The results included the effect of replacing flat plate absorber with new configurations (horizontal and longitudinal tubes) on the thermal performance of a double pass solar air heater. A comparison has been made between experimental and numerical results for validation. In addition to that, a comparison between the conventional and proposing systems has been presented.

4.1 Experimental and numerical validation

The validation between experimental and numerical work has been carried out as shown in Figs 6a to 6c. It can be observed that the deviation between experimental and numerical results ranges from 6.7% to 9.6% showing acceptable agreement.

4.2 Numerical results

4.2.1 Temperature distribution contours

The temperature distribution of airflow through the solar air heater for the three configurations has been presented in Figs. 7a- 7i. It is clearly shown from these figures that the temperature

of airflow rises as the flow moves forwards through the path of the collector's channels, and this increment is due to absorbed heat in the absorber which is transferred to airflow. In addition, it can be observed that reversing flow direction at the end of the lower channel leads to separating flow from the wall at the beginning of the upper channel, as well as creating vortices that enhance heat transfer via mixing the fluid flow. Moreover, the airflow temperature at the outlet decreases with increasing the mass flow rate as a result of lowering convection exchange with increasing airflow speed (Salih *et al.* 2019). Furthermore, it can be observed that the rising in the temperature of the airflow in the third configuration is higher than in the rest configurations due to increasing the heat transfer surface area. The temperature distribution for the absorber models is shown in

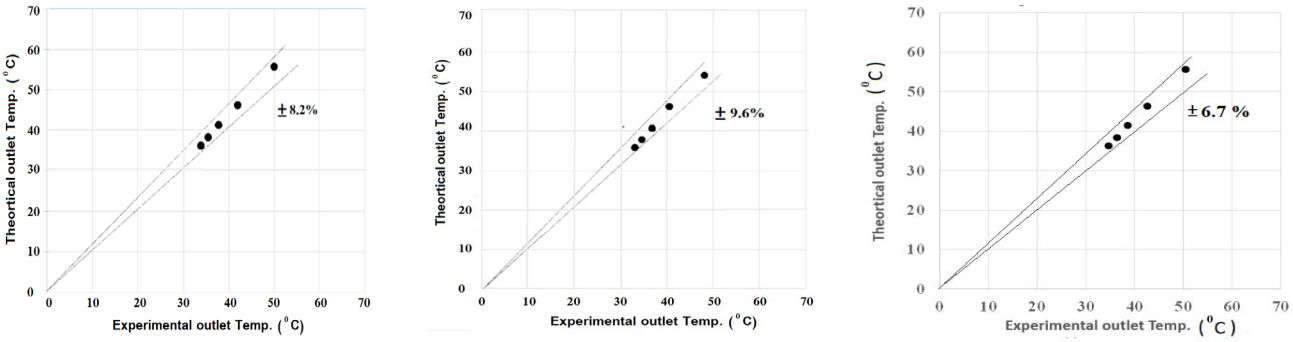

Fig. 6. (a) Validation between experimental and numerical results for DPSAHWFP, (b) Validation between experimental and numerical results for DPSAHWT-1, (c) Validation between experimental and numerical results for DPSAHWT-2 .

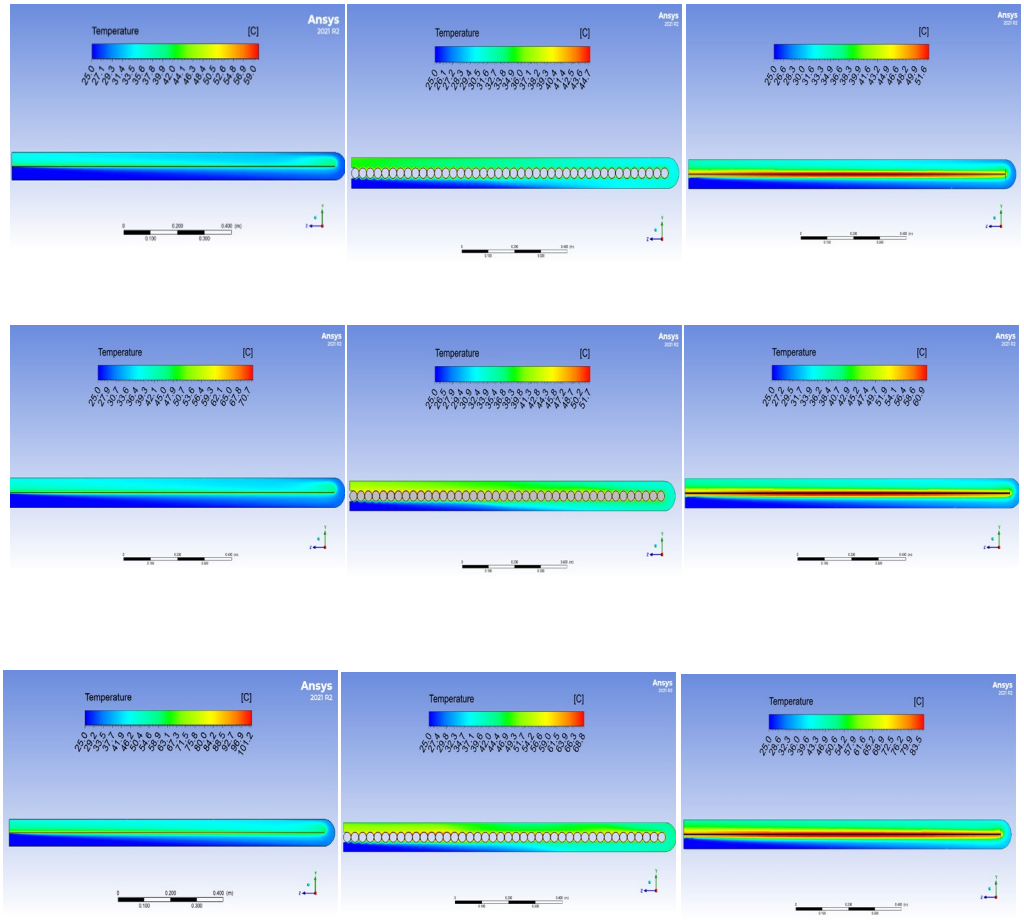

Figs. 7a-i. Temperature distribution of airflow along the double pass solar air heaters.

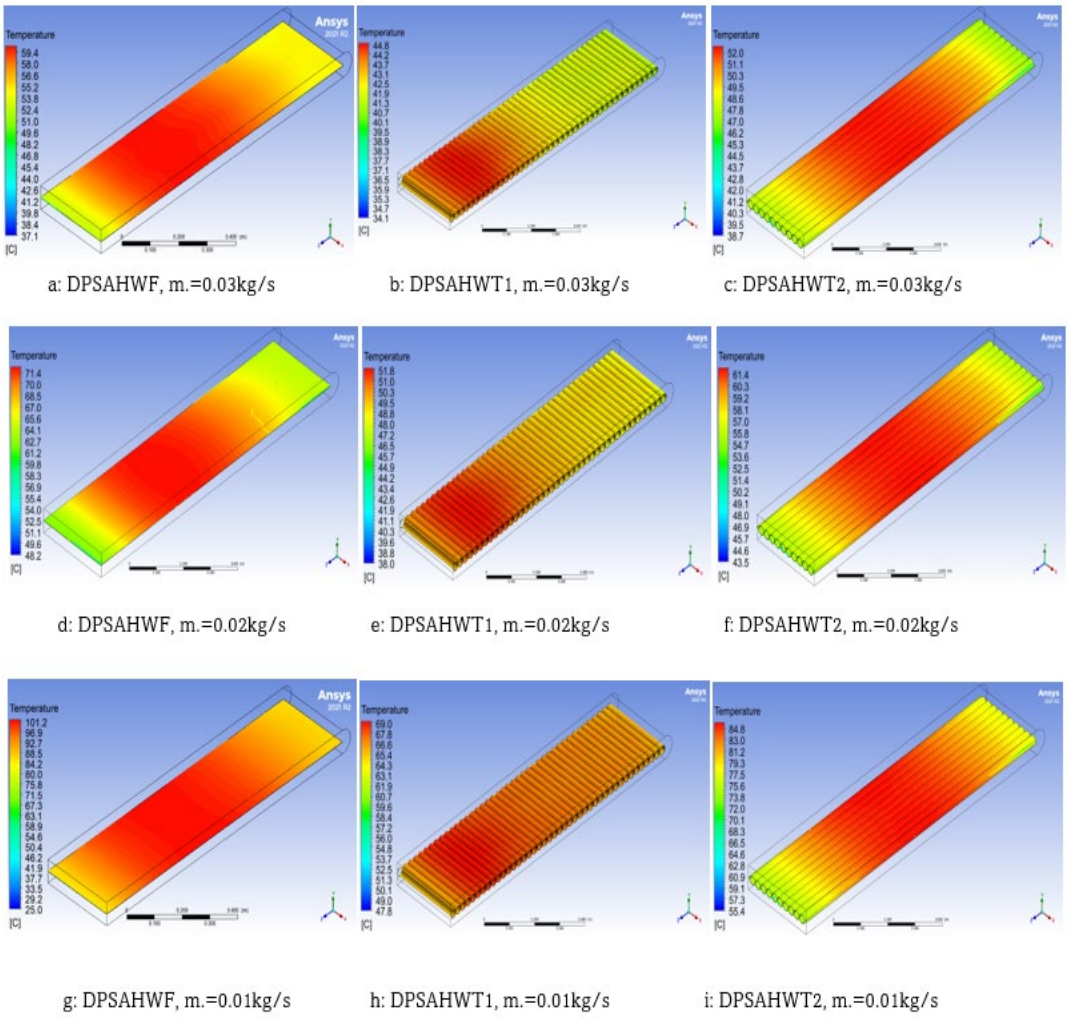

Figs. 8a-i. Temperature distribution of the absorber models.

Figs. 8a-i. The temperature distribution for all absorber models is observed to increase towards the middle of the solar collector, then decreases beyond this point towards the end of the collector, and this decrease is due to the vortices which are created at the upper channel that cause mixing up the airflow and increasing the heat transfer rate between airflow and absorber (Mohammed 2017). Moreover, as shown in these figures, there is an inverse relationship between increasing airflow rate and absorber temperature.

4.2.2. Air velocity vectors

A comparison between the three configurations in terms of velocity vector has been presented in Figs 9a-i for different mass flow rates. As observed from these figures, the location of maximum velocity at the end of the lower channel, and the flow separate at the beginning of the upper channel, and this separation increases as the air mass flow rate increases (Hussain *et al.* 2021).

4.3 Experimental results

4.3.1 Temperature variation of airflow

Figures 10a-i present the dimensionless temperature distribution of airflow through collector's channels for three selective values of air mass flowrates (0.01, 0.02, and 0.03) kg/s. In these figures, the temperature profile of airflow is described along the solar air heater's path. The airflow enters the lower channel i.e., between the backplate and the lower face of the absorber, then, the airflow recycles toward the upper channel i.e., between the upper face of the absorber and the glass cover. In general, it can be observed a gradual increment in all temperature curves from the collector's inlet to its outlet, and this increment can be attributed to the absorbed energy in the solar absorber which is transferred to airflow by convection (Handoyo and Ichsani 2016).

Figure 11 shows the influence of varying air mass flowrate on the temperature rise of airflow (Tair,out-Tair,in). It was noted that the temperature of airflow increases as the mass flow rate decreases, and this result can be attributed to the increase in the period time of passing air through the solar air heater's channels, which leads to making the air able to carry more thermal energy from the surface of solar absorber (Mahmood 2020).

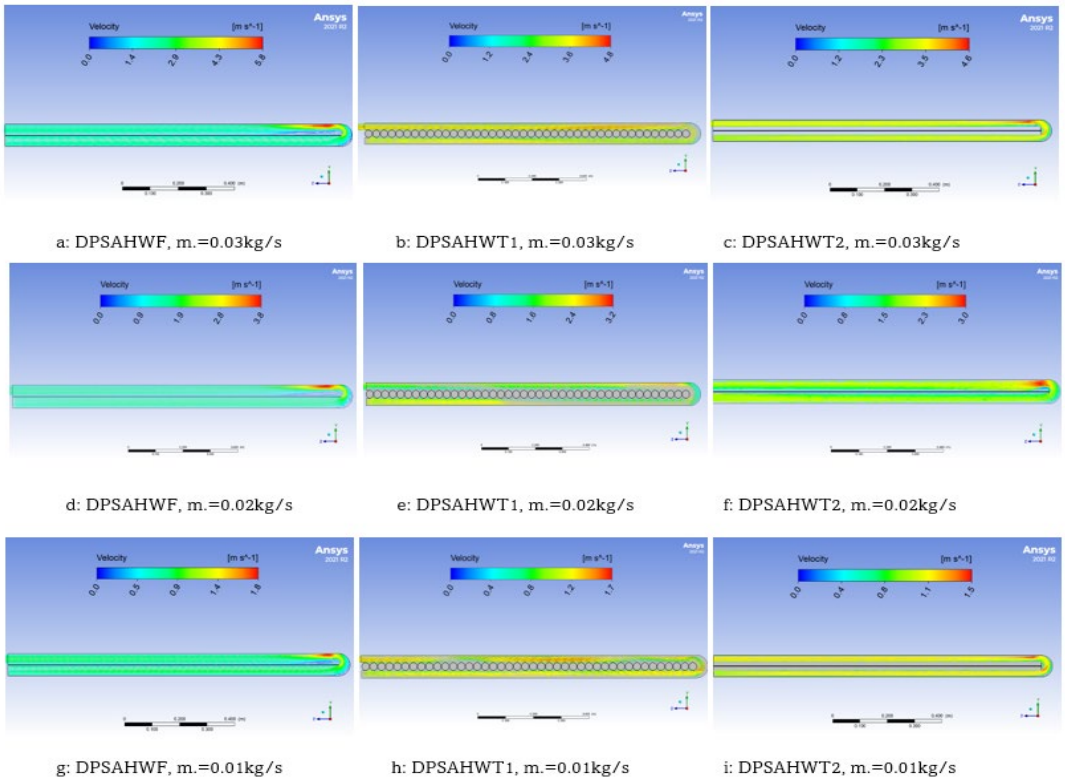

Figs. 9a-i. Velocity vectors of airflow through double pass solar air heaters

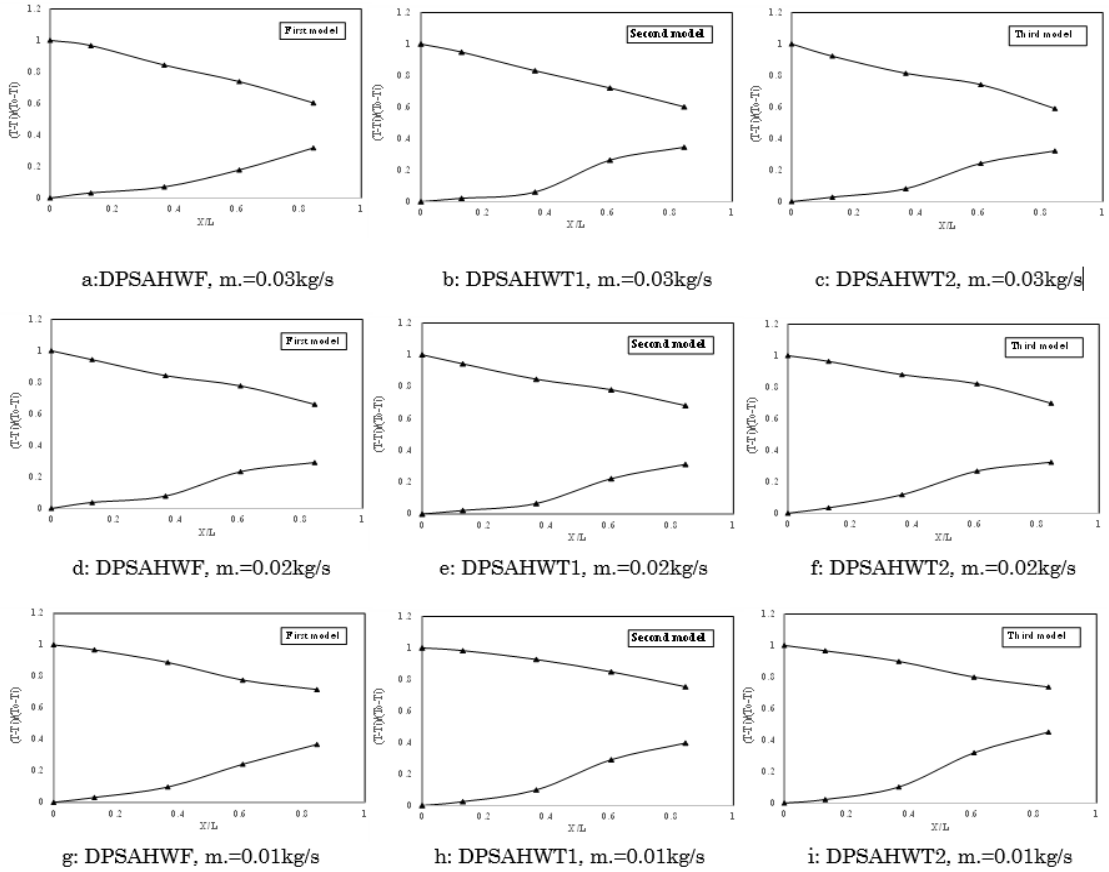

Figs. 10a-i. Temperature variation of airflow along lower& upper channels of double pass solar air heater

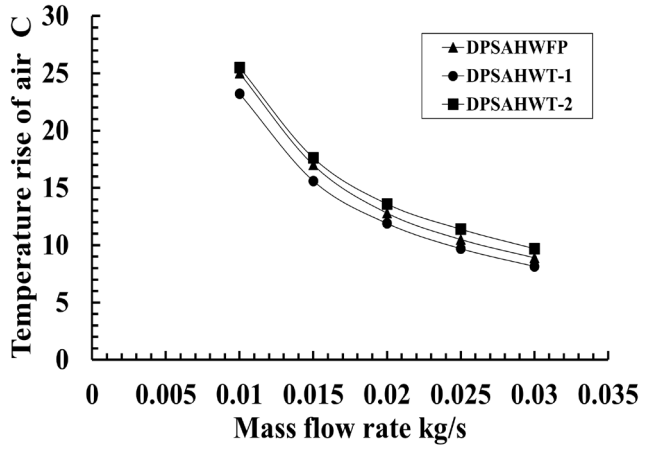

Fig. 11. Temperature rise of airflow (Tair, out-Tair, in) for different mass flow rates.

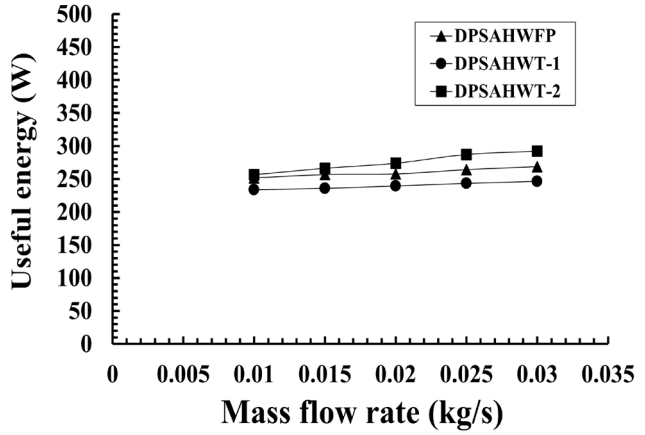

Fig. 12. Useful energy for different mass flow rates.

4.3.2. Useful energy rate and effective efficiency

For demonstrating the performance of the three configurations, the useful energy gain at different mass flow rates has been presented in Fig.12. It is clear from this figure that the amount of useful energy is directly proportional to the value of air mass flow rate (based on Eq. 2).

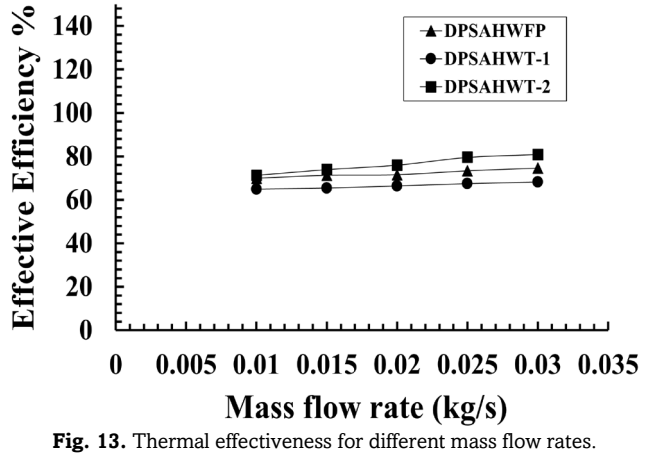

Fig. 13. Thermal effectiveness for different mass flow rates.

The maximum useful energy gain that equals (292 W) has been achieved at an airflow rate of 0.03 kg/s by the DPSAHWT-2, although the outlet air temperature rise at this mass flow rate value is less than other values, and this is mainly due to dominating effect of Reynolds number that leads to increasing convective heat transfer rate, hence, capturing more thermal energy from solar absorber's surface (Abo-Elfadl *et al.* 2021b).

To test the influence of pressure drop on the solar air heater's performance for the three configurations models, the effective efficiency or thermo-hydraulic efficiency of each configuration was calculated, and the outcomes are presented in fig. 13. Once again, the type of relationship between airflow rate and the effective efficiency is a positive relationship (i.e., effective efficiency increases with rising airflow rate value). This result can be attributed to increasing the gaining of useful energy by increasing the mass flow rate (Salih *et al.* 2019a). Moreover, the third configuration (DPSAHWT-2) has shown the highest effective efficiency (80.9%) at an airflow rate of 0.03 kg/s, and it is more efficient than the first and second models by 4.2 % and 9.8 % respectively.

5. Conclusions

In this work, conventional flat plate absorber has been replaced with tubular absorber. Furthermore, the influence of the tubes' direction with respect to airflow direction has been investigated. The results showed that the rising in air mass flow rate leads to reducing the residence time of air through the collector's channels which negatively affects the heat absorption from for absorber, thus decreasing the temperature rise of air (Tair,out-Tair,in). Moreover, and based on the air temperature rise (Tair,out-Tair,in), the amount of air that passes through the collector's channels has a remarkable impact on useful energy gain, although the air temperature rise is lower at the highest air mass flow rate, but the amount of useful energy gain is the highest. In addition, the maximum useful energy gain of (292 W) has been achieved at an air mass flow rate of 0.03 kg/s by the third configuration (DPSAHWT-2), while the lowest useful energy gain was in the second configuration (DPSAHWT-1) for the same mass flow rate.Moreover, the third configuration (DPSAHWT-2) offers better thermal performance than the other configurations, where the effective efficiency of this configuration is higher by 4.2% and 9.8 % than the first and second configurations respectively.

Acknowledgment

The authors thank the University of Technology- Iraq for providing help in completing this work.

Nomenclature

A_c	Collector area, m^2.
Cp_{air}	Specific energy of air, J/kg. ^{0} K.
E	Total energy of the fluid.
I	Solar radiation, W/m^2.
k_{eff}	Effective conductivity J/mk.
$\dot{m}_{air}$	Air mass flow rate, kg/s.
P	Pressure drop, Pa.
P_{air}	Air density, kg/m^3.
Q_{in}	Received energy, W.
$Q_{mechanecal}$	Pumping power, W.
Q_{out}	Useful energy gain, W.

$T_{air,in}$ Inlet air temperature, ^{0} C.
$T_{air,out}$ Outlet air temperature, ^{0} C.
W_R Total uncertainty.
W_n Uncertainty of independent variables.
x_n Independent variables.
η_{th} Thermal efficiency.
η_{eff} Effective efficiency.

References

Abed, A.H. (2016). Thermal storage efficiency enhancement for solar air heater using a combined SHSm and PCM cylindrical capsules system: experimental investigation. *Engineering and Technology Journal*, 34(5), 999-1011.

Abdelkader, T.K., Y. Zhang, E.S. Gaballah, S. Wang, Q. Wan, and Fan, Q. (2020). Energy and exergy analysis of a flat-plate solar air heater coated with carbon nanotubes and cupric oxide nanoparticles embedded in black paint. *Journal of Cleaner Production,* 250,119501; https://doi.org/10.1016/j.jclepro.2019.119501

Abdu, Y. (2021). Experimental Performance Investigation of Double Pass Solar Air Heater with Baffles for Red Chilli Drying. Ph.D. diss., ASTU.

Abo-Elfadl, S., M.S. Yousef, and Hassan, H. (2021a). Energy, exergy, and enviroeconomic assessment of double and single pass solar air heaters having a new design absorber. *Process Safety and Environmental Protection,* 149, 451-464; https://doi.org/10.1016/j.psep.2020.11.020.

Abo-Elfadl, S., M.F. El-Dosoky and Hassan, H. (2021b). Energy and exergy assessment of new designed solar air heater of V-shaped transverse finned absorber at single-and double-pass flow conditions. *Environmental Science and Pollution Research*, 28(48), 69074-69092; https://doi.org/10.1007/s11356-021-15163-z.

Akhbari, M., A. Rahimi, and Hatamipour, M. (2020). Modeling and experimental study of a triangular channel solar air heater. *Applied Thermal Engineering*, 170, 1-42; https://doi.org/10.1016/j.applthermaleng.2020.114902.

Alic, E., M. Das, and Akpinar, E.K. (2021). Design, manufacturing, numerical analysis and environmental effects of single-pass forced convection solar air collector. *Journal of Cleaner Production*, 311, 1-13; https://doi.org/10.1016/j.jclepro.2021.127518.

Assadeg, J., A.H. Al-Waeli, A. Fudholi, and Sopian, K. (2021). Energetic and exergetic analysis of a new double pass solar air collector with fins and phase change material. *Solar Energy*, 226, 260-271; https://doi.org/10.1016/j.solener.2021.08.056.

Bensaci, C.E. (2021). Effect of the artificial roughness dispositions on the thermal exchanges in a flat solar collector. Doctoral dissertation, Université Mohamed Khider–Biskra.

Das, B., J.D. Mondol, S. Debnath, A. Pugsley, M. Smyth, and Zacharopoulos, A. (2020). Effect of the absorber surface roughness on the performance of a solar air collector: *An experimental investigation. Renewable Energy,* 152, 567-578; https://doi.org/10.1016/j.renene.2020.01.056.

Dhiman, P., N.S. Thakur, and Chauhan, S. (2012). Thermal and thermohydraulic performance of counter and parallel flow packed bed solar air heaters. *Renewable Energy*, 46, 259-268; https://doi.org/10.1016/j.renene.2012.03.032.

El-Sebaii A., S. Aboul-Enein, M. Ramadan, S. Shalaby, and Moharram, B. (2011). Investigation of thermal performance of-double pass-flat and v-corrugated plate solar air heaters. *Energy*, 36, 1076-1086; http://dx.doi.org/10.1016/j.energy.2010.11.042.

Erol, Ö. (2022). Analysis of the Performance of a Solar Air Heater with Different Configurations: Effect of Fins and Turbulators. *Heat Transfer Research*, 53(6), 45-59; DOI: 10.1615/HeatTransRes.2022041666.

Gopi, S., & Muraleedharan, C. (2021). Modelling and experimental studies on a double-pass hybrid photovoltaic-thermal solar air heater with vertical slats attached in the lower channel. International Journal of Ambient. *International Journal of Ambient Energy* , 1-11; https://doi.org/10.1080/01430750.2021.1918241.

Habib, N.A., A.J. Ali, M.T. Chaichan, and Kareem, M. (2021). Carbon nanotubes/paraffin wax nanocomposite for improving the performance of a solar air heating system. *Thermal Science and Engineering Progress,* 23, 1-11; https://doi.org/10.1016/j.tsep.2021.100877.

Heydari, A. and Mesgarpour, M. (2018). Experimental analysis and numerical modeling of solar air heater with helical flow path. *Solar Energy*, 162, 278-288; https://doi.org/10.1016/j.solener.2018.01.030.

Ho, C.D., H. Chang, C.F. Hsiao, and Y. Lin, (2021). Optimizing Thermal Efficiencies of Double-Pass Cross-Corrugated Solar Air Heaters on Various Configurations with External Recycling. Energies 14(13), 4019; https://doi.org/10.3390/en14134019.

Hussain, M.K., A.M. Rasham, and Alshadeedi, B.M. (2021). Finite Element Modeling Of Finned Double-Pass Solar Air Heaters, in: 4th International Conference on Energy Conservation and Efficiency (ICECE), IEEE, 1-6. https://doi.org/10.1109/ICECE51984.2021.9406296.

Hussien, S.Q., & Farhan, A.A. (2019). The effect of metal foam fins on the thermo-hydraulic performance of a solar air heater. *Int. J. Renew. Energy Res.,* 9, 840-847.

Handoyo, E.A., and Ichsani, D. (2016). Numerical studies on the effect of delta-shaped obstacles' spacing on the heat transfer and pressure drop in v-corrugated channel of solar air heater. *Solar Energy*, 131, 47-60. http://dx.doi.org/10.1016/j.solener.2016.02.031.

Jalil, J.M., R.F. Nothim, and Hameed M.M. (2021). Effect of Wavy Fins on Thermal Performance of Double Pass Solar Air Heater. *Engineering and Technology Journal*, 39(9), 1362-1368; http://doi.org/10.30684/etj.v39i9.1775.

Jasim Mahmood, A. (2020). Thermal evaluation of a double-pass unglazed solar air heater with perforated plate and wire mesh layers. *Sustainability*, 12, 1-15; https://doi.org/10.3390/su12093619.

Kanase–Patil, A.B., M.G. Gabhane, and Kokare, P.K. (2022). Heat transfer study of a double-pass counterflow solar air heater with porous media and multiple C-shaped roughness absorber. *Energy Sources, Part A: Recovery, Utilization, and Environmental Effects*, 1-14; https://doi.org/10.1080/15567036.2022.2035469.

Khanlari, A., A. Sözen, F. Afshari, C. Şirin, A. Tuncer, and Gungor, A. (2020). Drying municipal sewage sludge with v-groove triple-pass and quadruple-pass solar air heaters along with testing of a solar absorber drying chamber. *Science of The Total Environment,* 709, 1-34; https://doi.org/10.1016/j.scitotenv.2019.136198.

Khanmohammadi, S., H.A. Chaghakaboodi, and Musharavati, F.(2021). A new design of solar tower system amplified with a thermoelectric unit to produce distilled water and power. *Applied Thermal Engineering,* 197, 1-15; https://doi.org/10.1016/j.applthermaleng.2021.117406.

Shafiee, M., A.m. Farbeh, and Firoozzadeh, M. (2022). Experimental Study on Using Oil-Based Nanofluids in a Vacuumed Tube Solar Water Heater; Exergy Analysis. *International Journal of Ambient Energy*, (just-accepted), 1-24; https://doi.org/10.1080/01430750.2022.2073267.

Karimipour-Fard, P., and Beheshti, H. (2017). Performance enhancement and environmental impact analysis of a solar chimney power plant: Twenty-four-hour simulation in climate condition of isfahan province, iran. *International Journal of Engineering*, 30, 1260-1269; doi: 10.5829/ije.2017.30.08b.20.

Kumar, A., P. Bhandari, and Rawat, K.S. (2021a). Numerical Simulation of Solar Air Heater using Paraffin Wax-Aluminum Compound as Phase Changing Material. *Aptisi Transactions on Technopreneurship (ATT)*, 3(2), 164-170.

Kumar, P.G., K. Balaji, D. Sakthivadivel, V.S. Vigneswaran, M. Meikandan, and Velraj, R. (2019b). Effect of using low-cost thermal insulation material in a solar air heating system with a shot blasted V- 14 corrugated absorber plate. *Thermal Science and Engineering Progress*, 14, 1-10;https://doi.org/10.1016/j.tsep.2019.100403.

Kumar, P.G., D. Sakthivadivel, K. Balaji, M. Salman, and Kim, S. (2021c). Performance enhancement of a double-pass solar air heater with a shot-blasted absorber plate and winglets. *Journal of Mechanical*

Science and Technology, 35(6), 2743-2753; http://doi.org/10.1007/s12206-021-0544-x.

Mahmood, A. (2020). Thermal evaluation of a double-pass unglazed solar air heater with perforated plate and wire mesh layers. *Sustainability*, 12 (9), 2-15.

Mohammed, A. (2017). Study of Double Pass Solar Air Heater Integrated with A Thermal Storage Material. Ph.D. thesis, University of Technology, Baghdad, Iraq.

Mohammed, M.F., M.A. Eleiwi, and Kamil, K. (2021). Experimental Investigation of Thermal Performance of Improvement a Solar Air Heater with Metallic Fiber. *Energy Sources, Part A: Recovery, Utilization, and Environmental Effects*, 43(18), 2319-2338; https://doi.org/10.1080/15567036.2020.1833110.

Monna, S., R. Abdallah, A. Juaidi, A. Albatayneh, A.J. Zapata-Sierra, and Manzano-Agugliaro, F. (2022). Potential Electricity Production by Installing Photovoltaic Systems on the Rooftops of Residential Buildings in Jordan: An Approach to Climate Change Mitigation. *Energies*, 15(2), 1-15. https://doi.org/10.3390/en15020496.

Perwez, A. and Kumar, R. (2019). Thermal performance investigation of the flat and spherical dimple absorber plate solar air heaters. *Solar Energy*, 193, 309-323; https://doi.org/10.1016/j.solener.2019.09.066.

Rajarajeswari, K., P. Alok, and Sreekumar, A. (2018). Simulation and experimental investigation of fluid flow in porous and non-porous solar air heaters. *Solar Energy*, 171, 258-270; https://doi.org/10.1016/j.solener.2018.06.079.

Rajendran, V., H. Ramasubbu, K. Alagar, and Ramalingam, V. (2021). Performance analysis of domestic solar air heating system using V-shaped baffles–an experimental study. *Proceedings of the institution of mechanical engineers, part E: journal of process mechanical engineering*, 235(5), 1705-1717; http://uk.sagepub.com/en-gb/journals-permissions.

Razak, A.A., Z.A.A. Majid, W.H. Azmi, M.H. Ruslan, S. Choobchian, G. Najafi, and Sopian, K. (2016). Review on matrix thermal absorber designs for solar air collector. *Renewable and Sustainable Energy Reviews*, 64, 682-693; https://doi.org/10.1016/j.rser.2016.06.015.

Saboohi, Z., F. Ommi, E. Rahmani, T. Moradi, A. Fattahi, M. Delpisheh, and N. Karimi, (2022). The effect of sinusoidal fins' amplitude on the thermo-hydraulic performance of a solar air heater. *Chemical Engineering Communications*, 1-15; https://doi.org/10.1080/00986445.2022.2026338.

Salih, S.M., J.M. Jalil, and Najim, S.E. (2019a). Experimental and numerical analysis of double-pass solar air heater utilizing multiple capsules PCM. *Renewable Energy*, 143, 1053-1066; https://doi.org/10.1016/j.renene.2019.05.050.

Salih, M.M.M., O.R. Alomar, and Yassien, H.N.S. (2021b). Impacts of adding porous media on performance of double-pass solar air heater under natural and forced air circulation processes. *International Journal of Mechanical Sciences*, 210, 1-14; https://doi.org/10.1016/j.ijmecsci.2021.106738.

Salih, S.M., J.M. Jalil, and Najim, S.E. (2019c). Double-Pass Solar air Heater (DP-SAH) utilizing Latent Thermal Energy Storage (LTES). *In IOP Conference Series: Materials Science and Engineering*, 518 (3), 1-14; doi:10.1088/1757-899X/518/3/032038.

Salman, M., R. Chauhan, G. kumar Poongavanam, M.H. Park, and Kim, S. (2022). Utilizing jet impingement on protrusion/dimple heated plate to improve the performance of double pass solar heat collector. *Renewable Energy*, 181, 653-665; https://doi.org/10.1016/j.renene.2021.09.082.

Singh, R., P. Salhan, and Kumar, A. (2021). CFD Modelling and Simulation of an Indirect Forced Convection Solar Dryer. In IOP Conference Series. *Earth and Environmental Science*, 795(1), 1-9.

Singh, S., S.K. Chaurasiya, and Negi, B. (2021). Efficient design of a wavy channel embedded with porous media for solar air heating. *Energy Sources, Part A: Recovery, Utilization, and Environmental Effects*, 43(21), 2738-2754; https://doi.org/10.1080/15567036.2020.1850930.

Thakur, D.S., M.K., Khan, and Pathak, M. (2017). Solar air heater with hyperbolic ribs: 3D simulation with experimental validation. *Renewable Energy*, 113, 357-368; https://doi.org/10.1016/j.renene.2017.05.096.

Yadav, A.S. and Bhagoria, J.L. (2013). Modeling and simulation of turbulent flows through a solar air heater having square-sectioned transverse rib roughness on the absorber plate. *The Scientific World Journal, 2013, 1-12*; https://doi.org/10.1155/2013/827131.